Calculations of electronic excitation by protons and α particles in silicon

Luke W. Campbell
National Security Directorate, Pacific Northwest National Laboratory, Richland, Washington 99352, USA

(Received 19 September 2018; revised 12 August 2020; accepted 16 October 2020; published 2 December 2020)

This paper presents a method of calculating the valence electron contribution to the stopping and interaction cross sections of swift ions in matter using linear response calculations of the dielectric function in crystals. The *ab initio* response function is used to calculate excitations at low energy and momentum transfers to account for material-specific effects, while higher energy and momentum transfers use a free electron gas response for increased computational efficiency. The ECPSSR method for computing core cross sections is modified to allow predictions of the core contribution to electronic stopping. The charge distribution by entrained electrons is explicitly modeled to account for the additional screening beyond linear response. We use the methods developed to predict the electronic stopping of protons and α particles in silicon and compare to measured values.

DOI: 10.1103/PhysRevB.102.245103

I. INTRODUCTION

The response of condensed matter to the passage of charged particles has been a subject of interest to the physics community for more than a century. In the current age of Monte Carlo codes for simulating radiation transport [1,2], certain processes—nuclear interactions, some deep electronic core excitations, Rutherford scattering—are handled as discrete events, while others—valence and shallow electronic core interactions, phonon excitation—are approximated as continuous processes that slow the particle down as it traverses the sample. The latter type of process is often referred to as "stopping." These processes are traditionally handled with some variation of the Bethe formula [3], which is valid at relatively high particle energies and requires a single empirical material parameter, the mean atomic excitation energy, in addition to known values of the ion nuclear charge and material electron density. At lower ion speeds, below approximately one atomic unit of speed v_0, the Bethe formula loses validity and the Lindhard-Sharff-Schiott (or LSS) formula [4] is used, which requires a single empirical scaling parameter. In recent decades, Bethe and LSS stopping has been extended and combined with empirical data to give relatively accurate descriptions of energy loss, range, and straggling of ions in matter [5,6].

More recently, many attempts have been made to understand stopping using *ab initio* calculations in real materials. Among the earliest, Campillo, Pitarke, and their coworkers described using linear response calculations to predict the stopping of protons in aluminum [7,8] and silicon [9]. Later, Shukri *et al.* [10] similarly calculated the stopping of protons in aluminum and silicon under the linear response formalism, showing good agreement with data. They noted the challenges of converging the calculations with respect to the number of bands included in the calculation and the $\boldsymbol{k}$-point grid, and the importance of including core states in the calculations, as well as mentioning the significant additional computational cost to including them.

Linear response calculations are known to work well at high projectile ion speeds but are less accurate at low speeds—particularly for heavier ions, where entrained electrons (electrons that move with the ion in bound states) are not well represented. Previous work has investigated the stopping of ions in an electron gas at low speeds to all orders in the projectile nuclear charge, Z [11–14]. These works calculate the friction coefficient (stopping divided by ion speed) in the limit of vanishing projectile speed. These works report agreement with the variation in friction coefficient with changing Z. Their limitations are that they do not reproduce stopping at higher speeds and they rely on an electron gas description which can miss the effects of material properties. For example, attempts to extend the stopping theory to simulate radiation track structure will fail to reproduce the track ionization density in an insulator or semiconductor with an electron gas model, which lacks a band gap and will thus result in large numbers of unphysical excitations present within the material band gap.

An alternative approach uses real-time time-dependent density functional theory (RT-TDDFT) to explicitly simulate the time evolution of the electronic state as a charged projectile is moved through a lattice at constant speed. This method was used by Pruneda *et al.* [15] to calculate stopping of protons and antiprotons in lithium fluoride, by Yost and Kanai [16] to calculate stopping of protons and α particles in silicon carbide, and by Yost *et al.* [17] for protons in silicon. The RT-TDDFT method gives contributions to all orders, including those beyond linear response. However, it is computationally expensive, particularly if a representative sample of trajectories is to be averaged over.

This paper seeks to overcome some of the limitations of linear response calculations, while using much of the same computational machinery. We attempt to overcome the slow convergence by noting that at high energy or momentum transfer from the ion to the material, the forces of the material on its electrons can be neglected and an electron gas model will suffice for these kinds of excitations, reserving the

computationally more expensive integrations over the *ab initio* response function for low energy and low momentum transfer excitations. Core excitations will be dealt with using ECPSSR theory [18], which has proved successful in reproducing core-level cross sections but has not yet been applied to stopping. ECPSSR is much less computationally expensive than plane-wave calculations for atomic cores. Finally, we attempt to explore whether the limitations of linear response on stopping of slow ions with $Z > 1$ can be handled with an explicit model of the screening cloud of entrained electrons captured by the ion. This is conceptually similar to the "effective Z" model commonly used to estimate stopping [19,20]. This attempts to fill a need for rapid preliminary calculations of electronic excitations across a wide range of energies needed for radiation track structure simulations [21–23]. Because silicon has a wealth of experimental data associated with it, we choose to perform initial simulations on this material, using proton and α-particle projectiles.

Unless explicitly specified otherwise, throughout this document we use atomic units ($e = \hbar = m_e = 1$) for calculations and to develop theory. Results are presented in more accessible and familiar units.

II. THEORY

In this paper, we consider an ion moving through a crystalline and nonmetallic material. The temperature is low enough that the material can be approximated in its electronic ground state. The electrons occupy Bloch orbitals in band n and wave vector $\boldsymbol{k}$ denoted $\psi_{n,\boldsymbol{k}}(\boldsymbol{r})$ with eigenenergies $\varepsilon_n(\boldsymbol{k})$. Modern plane-wave electronic structure codes can efficiently calculate $\psi_{n,\boldsymbol{k}}(\boldsymbol{r})$ and $\varepsilon_n(\boldsymbol{k})$ [24–26].

We will pursue the following strategy. At high energy and momentum transfer between the ion and the material, the detailed nature of the bonding of the valence electron to the material does not matter much. Under these conditions, the electronic system can be treated to a good approximation as a free electron gas, allowing calculations to be performed rapidly and efficiently. At momentum transfer smaller than a given momentum cutoff magnitude q_{crit} and energy transfers smaller than an energy threshold ω_{crit}, the full nature of the material's electronic response will be required to describe the interaction, including the material band gap and interband transitions. To keep the calculations tractable, excitons and other effects beyond the random phase approximation (RPA) will be neglected. We will thus require separate descriptions of the screening and interaction in the high momentum or energy limit and the low energy and momentum limit.

A. Screening

Electronic losses arise from dynamical effects of the screening, which is the electronic response of the material to a perturbing charge.

1. Ab initio screening

Adler and Wiser [27,28] independently derived the dielectric function of a crystal in the RPA, in a form that can be calculated with the Bloch orbitals and eigenenergies. The dielectric response $\epsilon_{\boldsymbol{K},\boldsymbol{K}'}(\boldsymbol{q}_B, \omega)$ is a 3-tensor valued function that is also a matrix in the space of reciprocal lattice vectors $\boldsymbol{K}, \boldsymbol{K}'$. (Here, $\boldsymbol{q}_B$ is the wave number confined to the first Brillouin zone and ω is the energy transfer. In order to make the notation more compact, we use $\boldsymbol{q} = \boldsymbol{q}_B + \boldsymbol{K}$ elsewhere in this paper for the total momentum transfer.) The functional form of ϵ is reviewed in Appendix A. For isotropic materials, the spatial tensor aspect of the function can be neglected but finding the inverse dielectric function still requires a matrix inverse in the space of inverse lattice vectors.

2. Free electron gas screening

Lindhard [29,30] has developed the dielectric response of the homogeneous free electron gas. Because the material is assumed homogeneous and isotropic, the dielectric function is scalar and diagonal in the lattice vectors $\boldsymbol{K}$. The response is described with a single momentum transfer variable spanning all possible momenta $\epsilon(\boldsymbol{q}, \omega)$, where $\boldsymbol{q}$ is no longer restricted to the first Brillouin zone. The inverse dielectric function is a simple reciprocal rather than a matrix inverse.

B. Rate of loss

As detailed in Appendix B, the interaction rate can be found by

$$\Gamma(\boldsymbol{v}) = 2\int_0^\infty d\omega \sum_{\boldsymbol{K}} \int \frac{d^3q_B}{8\pi^3} \frac{4\pi}{|\boldsymbol{q}|^2} |\rho_a(\boldsymbol{q})|^2 \mathcal{L}_{\boldsymbol{K}\boldsymbol{K}}(\boldsymbol{q}_B, \omega)\, \delta\left(\omega - \boldsymbol{q}\cdot\boldsymbol{v} + \frac{|\boldsymbol{q}|^2}{2M}\right), \tag{1}$$

where $\rho_a(\boldsymbol{q})$ is the Fourier transform of the atom's charge distribution and $\mathcal{L}_{\boldsymbol{K}\boldsymbol{K}'}(\boldsymbol{q}_B, \omega)$ is the loss function of the material [$-i$ times the anti-Hermitian part of $\epsilon^{-1}_{\boldsymbol{K},\boldsymbol{K}'}(\boldsymbol{q}_B, \omega)$]. The energy loss rate is given by a similar equation, differing only by weighting the integrand by a factor of the energy transfer ω:

$$\dot{E}(\boldsymbol{v}) = 2\int_0^\infty d\omega\, \omega \sum_{\boldsymbol{K}} \int \frac{d^3q_B}{8\pi^3} \frac{4\pi}{|\boldsymbol{q}|^2} |\rho_a(\boldsymbol{q})|^2 \mathcal{L}_{\boldsymbol{K}\boldsymbol{K}}(\boldsymbol{q}_B, \omega)\, \delta\left(\omega - \boldsymbol{q}\cdot\boldsymbol{v} + \frac{|\boldsymbol{q}|^2}{2M}\right). \tag{2}$$

For a spherically symmetric charge distribution in an isotropic homogeneous material, the expression for the scattering rate and rate of energy loss simplify

$$\Gamma(\boldsymbol{v}) = \frac{2}{\pi v}\int_0^{2Mv} \frac{dq}{q} |\rho_a(q)|^2 \int_0^{\omega_+} d\omega \left|\operatorname{Im}\epsilon^{-1}(q,\omega)\right|, \tag{3}$$

$$\dot{E}(\boldsymbol{v}) = \frac{2}{\pi v}\int_0^{2Mv} \frac{dq}{q} |\rho_a(q)|^2 \int_0^{\omega_+} d\omega\, \omega \left|\operatorname{Im}\epsilon^{-1}(q,\omega)\right|, \tag{4}$$

where $\omega_+ = qv - q^2/2M$, which can be exploited when using free electron gas representations of the response.

These expressions [Eqs. (1)–(4)] for the scattering and energy loss rates are valid in the nonrelativistic limit. To find the stopping of ions moving at a significant fraction of the speed of light, relativistic corrections will need to be included.

To convert from rates to interactions (or energy loss) per distance traveled, divide by the ion's speed. The inverse mean free path between interaction events is thus

$$\lambda^{-1}(\boldsymbol{v}) = \frac{\Gamma(\boldsymbol{v})}{v} \tag{5}$$

and the stopping (energy loss per distance traveled) [31] is

$$S(\boldsymbol{v}) = \frac{\dot{E}}{v}. \tag{6}$$

The inverse mean free path is related to the cross section for interaction σ through the density of interaction centers N/V

$$\lambda^{-1}(\boldsymbol{v}) = \sigma(\boldsymbol{v})N/V. \tag{7}$$

Thus, we obtain the formula for electronic excitation cross sections

$$\sigma(\boldsymbol{v}) = \frac{\Gamma(\boldsymbol{v})}{v}\frac{V}{N}. \tag{8}$$

It should be noted that some ambiguity may occur in the natural choice of what constitutes an interaction center. For core shell ionization, the clear choice is an individual atom. The valence electrons, however, are much more delocalized throughout the material to the extent that the free electron gas approximation has no natural choice for an interaction center. The cross section can be chosen to be per atom, per crystallographic unit cell, or per chemical unit (e.g., one strontium atom and two iodine atoms for SrI_2). This is merely a convention, as the choice of how to conceptually divide up the lattice can have no effect on observables. In this work, we chose to use the crystallographic unit cell of the silicon lattice as the interaction center for defining valence cross sections.

C. Core-level excitations

In principle, the above methods for finding the material screening could be used to compute the excitations of core electronic states to conduction states. In practice, core states are prohibitively expensive to compute using plane-wave electronic structure codes. We assume that the electronic bands can be separated into core and valence states. The scattering and loss rates of the valence states can be handled as above. Core excitation cross sections by light ions have been found to be accurately modeled using the ECPSSR (stands for (E) Energy-loss effect, (C) Coulomb repulsion, (PSS) Perturbed Stationary States, and (R) Relativistic) method [18], which adds corrections to the plane-wave Born approximation (PWBA) scattering cross sections of screened hydrogenic states of the target atoms. These corrections account for the curved trajectory of the projectile in the field of the atomic nucleus and deep core states, screening by core electronic states, and the increased binding energy of the core state when the projectile nucleus is very close to the target nucleus.

ECPSSR is usually used for the calculation of core ionization cross sections. With a small modification, it can also produce the stopping due to core excitations. A review of ECPSSR theory and the modification to allow stopping calculations is given in Appendix C. It must be noted that if the material contains heavy atoms with N, O, or P core shells, additional work will need to be done to parametrize the PWBA expressions for those shells.

III. CALCULATIONS

The integrals in Eqs. (3), (4), and (C6) are evaluated using Gauss three-point quadrature over an adaptive grid, subdividing portions of the grid until the integral in each section is converged. In all cases, the numerical effort to evaluate the integrals was negligible compared to the integration of the valence loss rates and cross sections (below).

The ground-state wave function of silicon was calculated using the ABINIT plane-wave electronic structure code [24]. A lattice parameter of 10.217 Bohr radii was used, and the orbitals calculated on a $10 \times 10 \times 10$ $\boldsymbol{k}$-point grid in the first Brillouin zone. The $3s$ and $3p$ valence electrons were included in the calculations; the silicon core was represented with a norm-conserving pseudopotential generated with the ONCVPSP code [32] available from the ABINIT website. The electronic structure was converged with a 20-Hartree plane-wave cutoff.

The *ab initio* dielectric response of Eq. (A1) was calculated using the Kohn-Sham orbitals and eigenvalues from the ground-state results, integrated on the $\boldsymbol{k}$-point grid of the ground-state calculation using the tetrahedron method [33]. The response was tabulated from 0 to 100 eV at 0.1-eV steps, with $\boldsymbol{q}$ points on the $10 \times 10 \times 10$ grid from the ground-state calculations. A cutoff of 10 Hartree was chosen for cutoff of reciprocal lattice vector energies to represent the exchange and correlation contributions; off-diagonal (local field) plane waves were calculated for the dielectric matrix with a plane-wave energy cutoff of 1 Hartree. A scissors operator was chosen to enforce a band gap of 1.125 eV.

The ion charge distribution $\rho_a(\boldsymbol{q})$ is estimated using the Brandt and Kitagawa model [19], with the energy stripping criterion of Mathar and Posselt [20]. Because previous work reported that linear response calculations are in agreement with commonly accepted stopping values for protons in matter [10], it is likely that the polarization cloud around a proton as calculated by linear response is similar to the actual cloud of entrained electrons carried by the proton as bound states. If this is the case, the relevant screening charge distribution will be the ion charge distribution as calculated by the Brandt-Kitagawa model minus Z times the electron charge distribution of a Brandt-Kitagawa proton, which will give the excess screening charge beyond what is produced by linear response. This is referred to as the "corrected screening" model in this paper.

For momentum transfer magnitudes above approximately $q = 2\ a_0^{-1}$, with a_0 as the Bohr radius, the calculated *ab initio* response function for silicon is reasonably well approximated by the electron gas response function, as shown in Fig. 1. For momentum transfers below approximately $q = 2\ a_0^{-1}$, the response function becomes negligibly small above

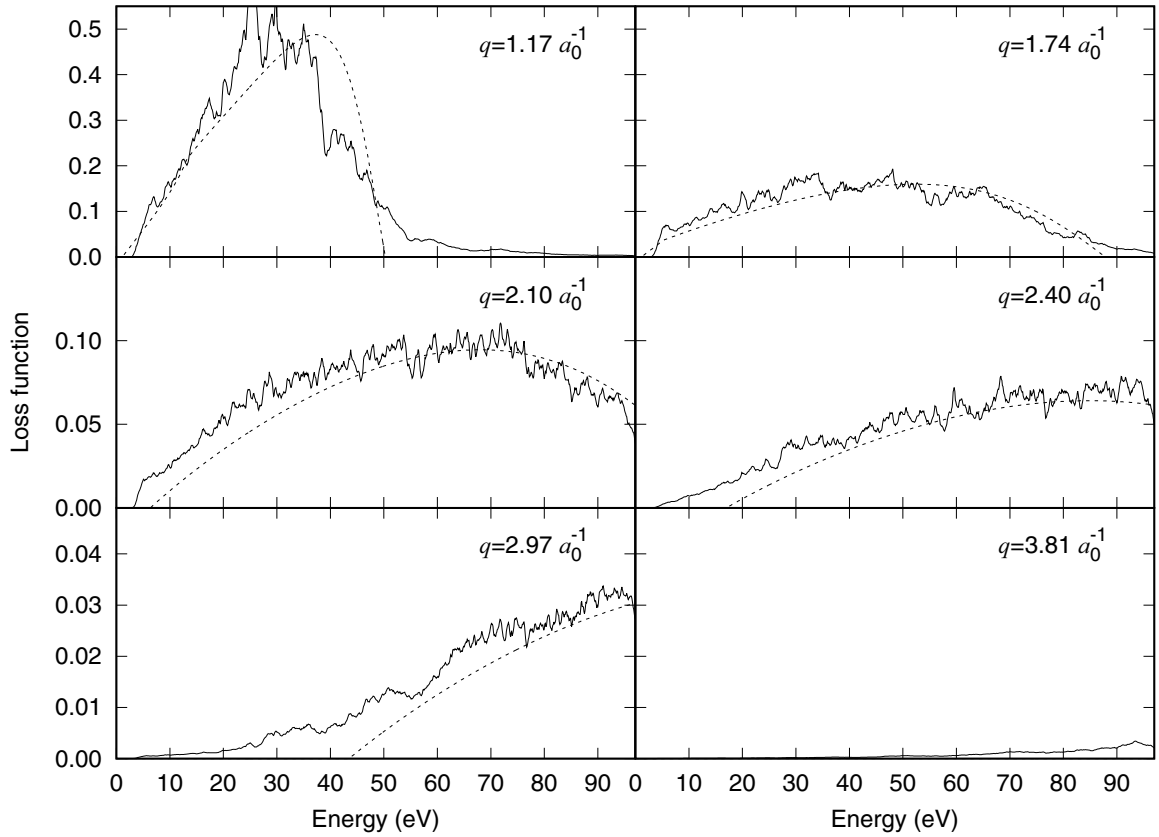

FIG. 1. The *ab initio* calculated diagonal loss function (solid lines) compared to the free electron gas approximation (dashed lines).

approximately 80 eV. The "cutoff" $q = 2\ a_0^{-1}$ and $\omega = 80$ eV chosen by eye will need to be adjusted to reach adequate numerical convergence. We therefore choose the following method to separate integration over an electron gas response function from that over the *ab initio* response function. For momentum transfers of less than $q_{\text{crit}} = 3.5\ a_0^{-1}$ and energy transfers of less than $\omega_{\text{crit}} = 100$ eV, tetrahedron integration is used to evaluate the scattering rate integral Eq. (1) and energy loss rate integral Eq. (2) on a grid spacing given by the dielectric response calculation grid. These choices for q_{crit} and ω_{crit} were found to be well converged. Where it has been calculated, the *ab initio* calculated response function for the silicon crystal was used in these integrals; outside of this region, the free electron gas response was used to fill in the space between the filled cube in reciprocal space of tabulated *ab initio* response and the momentum space cut-off sphere at q_{crit}. For energy or momentum transfers outside of the cut-off thresholds, Eqs. (3) and (4) are used with the free electron gas form of the response. This procedure avoids the slow convergence with respect to bands and dielectric matrix cutoff energies mentioned in Ref. [10].

It is useful to compare our methods with commonly used approximations. For comparison of our predictions with the widely used Bethe formula, we used the following function:

$$S_{\text{Bethe}}(v) = \frac{4\pi Z^2 e^4 \rho_e}{m_e v^2} \ln\left[\frac{2m_e v^2}{I}\right], \tag{9}$$

where m_e is the electron mass, e is the elementary charge, and I is the mean excitation energy of the material (taken as 173 eV for Si). At high ion speeds, our calculations should converge with the Bethe formula. The form of the Bethe equation shown here, and used in this work, is valid at nonrelativistic speeds and neglects the Barkas-Anderson corrections, Bloch corrections, and shell corrections. Although these corrections and the inclusion of relativistic effects can be important for accurate comparisons in some speed ranges, they will not qualitatively affect our results where it is used for comparison in the high but not relativistic ion speed range.

IV. RESULTS

Core excitation cross sections are compared to previously published data in Fig. 2. The K-shell cross sections are in good agreement with measurements; the predicted L-shell cross sections lie at the upper range of the data error bars. It is not clear if the L-shell measurements are low, or if the ECPSSR theory over-predicts the cross sections by about 20%. Archubi and Arista [34] have also calculated core cross sections for protons in silicon using a separate method; ECPSSR provides a better match to the measured data of silicon core excitation cross sections by protons than the EWPM method of these authors. That the core shell cross sections can be adequately calculated is not surprising, because the ECPSSR theory is already well established for this purpose and not novel to this study. Our results merely demonstrate this theory on silicon to illustrate how core excitations can be handled and accounted for.

Figure 3 shows our predictions for the valence stopping of protons in silicon compared to similar calculations made

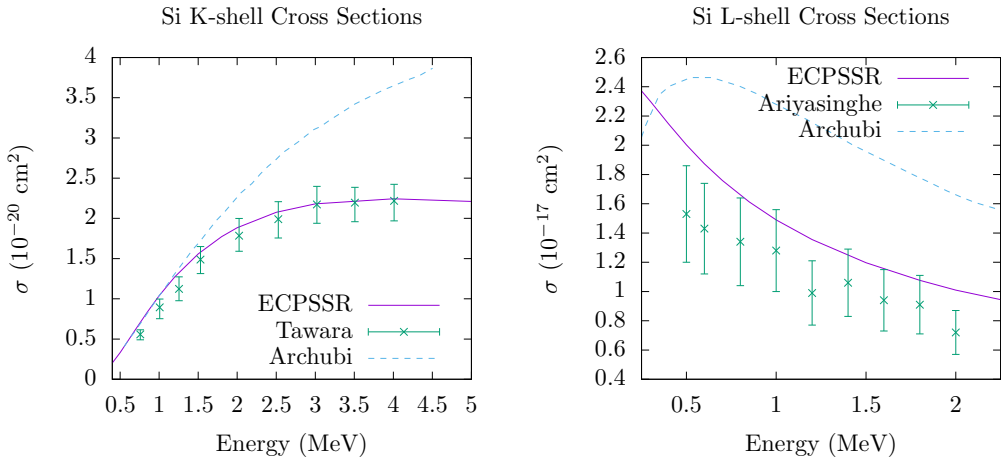

FIG. 2. Core excitation cross sections of protons in silicon, comparing the ECPSSR theory (purple solid line) to data (green × symbols, with error bars) and the EWPM calculations of Archubi and Arista [34] (blue dashed line). Left: K-shell cross sections, with data from Tawara *et al.* [35] Right: combined L-shell cross sections, with data from Ariyasinghe *et al.* [36].

by others. It is notable that the real-time TDDFT approach of Yost *et al.* [17] lies close to the linear response calculations of Shukri *et al.* [10] and those of this work that treat the proton as a point particle. Meanwhile, our model, which explicitly includes the charge cloud of entrained electrons using the Brandt-Kitagawa model, gives results significantly below the other predictions. It is noteworthy that the RT-TDDFT calculations, which take screening at all orders into account, already include the cloud of entrained electrons around the proton. This offers some evidence that, as previously suggested, linear response already does an adequate job of approximating the screening of protons at typical material electron densities.

The calculated stopping of protons is compared to measured data in Fig. 4. For α particles, our predictions are compared to measured data in Fig. 5. Note that only the data from Grahmann and Kalbitzer [39] is for electronic stopping alone; the rest also has contributions from nuclear stopping. At high speeds, the stopping of an ion is expected to be mostly electronic in nature. Thus, for high-energy particles, the total stopping should be a good measure of the electronic stopping. Although at lower speeds nuclear stopping becomes more significant, the effect of nuclear stopping is expected to be small over the range of energies for which we have data, on the order of 1% for protons in silicon [45] and 20% for α particles in silicon [46] at 10 keV and decreasing at higher energies. For the data shown in Fig. 4, this small discrepancy means that nuclear stopping alone cannot explain the difference between the trends seen in the total stopping data of Kührt *et al.* or that of Mertens and Bauwer compared to the electronic-only stopping of Grahmann and Kalbitzer. Given that the linear response calculations of this work for electronic stopping of protons give good agreement with calculations of other authors that take screening of all orders into account, as shown in Fig. 3, and that our linear response calculations also show good agreement with the total stopping measurements at energy ranges where nuclear stopping is expected to be negligible, it is likely that the agreement of our screened calculations with the data of Grahmann and Kalbitzer is a coincidence.

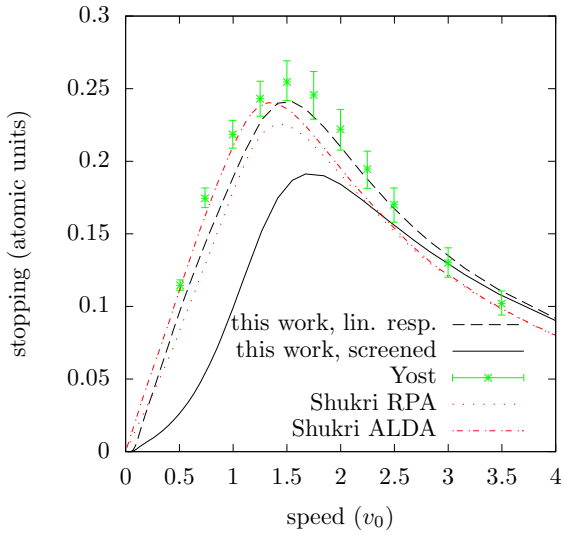

FIG. 3. A comparison of theoretical studies. Valence stopping from linear response only (dashed line) and with Brant-Kitagawa screening (full line), compared to RT-TDDFT valence stopping from Yost *et al.* [17] (green stars with error bars) and to the valence RPA (red dots) and ALDA (red dash-dots) results of Shukri *et al.* [10].

The contributions of valence, L-shell core states, and K-shell core states to the electronic cross sections and stopping of protons and α particles are shown in Fig. 6. Over most of the energy range studied, the valence electrons have the dominant effect. At high energies, L-shell excitations come to dominate the stopping if not the cross sections. This can be understood because each individual L-shell excitation transfers significantly more energy to the excited electron than the valence excitations. Over the energy range simulated here, the K-shell contributions of silicon are negligible.

The general behavior of the total cross sections and stopping curves in Fig. 6 are similar. They vanish at low energies where kinematic constraints force high-energy transfers to occur at high-momentum transfers where the loss function is very small. The presence of the band gap disallows small

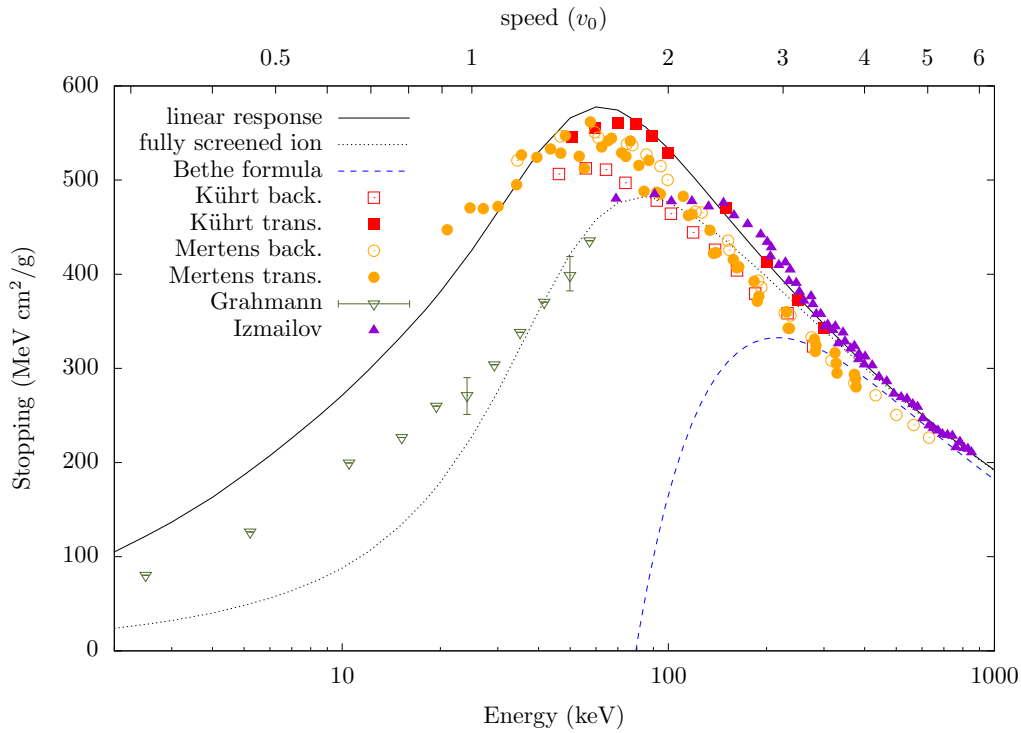

FIG. 4. Total predicted electronic stopping of protons particles in silicon for basic linear response theory (black solid line) and with ion screening from entrained electrons (black dotted line), compared to the Bethe (blue double-dot-dashed line) formula and to measured data by Kührt *et al.* [37] (red open squares for backscatter, red filled squares for transmission); Mertens and Bauer [38] (orange open circles for backscatter, orange filled circles for transmission); Grahmann and Kalbitzer [39] (dark green open inverted triangles); and Izmailov *et al.* [40] (purple closed inverted triangles). Of the measured data, only that of Grahmann and Kalbitzer is for electronic stopping; all others measure total stopping.

energy-transfer interactions, thus explaining the low stopping and cross sections at these energies. At slightly higher energies, the cross section and stopping increase with energy before rising to go through a maximum and then begin decreasing with increasing energy.

V. DISCUSSION

The development of a generally applicable theory that describes both fast and slow projectile ions in a material is challenging. Our approach relies on a simplified model of screening to represent the additional charge around an ion beyond that given by linear screening. The results suggest that this simple screening distribution improves the stopping calculations for α particles. In principle, this method could be applied to heavier ions to model the effect of their bound electrons on their electronic screening. However, further validation of entrained screening models is needed against heavier ions than α particles before it can be fully accepted. Clearly, the accuracy of the charge distribution model will also affect the calculated stopping. A more sophisticated model using first-principles calculations of the electronic structure of atoms in various charge states could produce improved performance.

An alternate method for simulating the stopping across large energy ranges and nuclear charges would be to extend the friction coefficient calculations mentioned in the introduction [11–14] to cover higher energies. Although beyond the scope of this paper, it is worth noting that if Eq. (2) is modified to sum over local fields (that is, including $\boldsymbol{K}$ and $\boldsymbol{K}'$ in the sum and including off-diagonal elements of the loss function), it can be reworked to be identical to Eq. (10) of the paper by Nazarov *et al.* [14] in the limit of low ω. Thus, using the same density functional as was used to obtain the friction coefficients would return the same low-energy behavior in stopping calculations if local fields are included, while the high-energy behavior would be expected to remain relatively accurate; consequently, it is possible that such an approach would give a good prediction of the stopping over all energies and nuclear charges.

At sufficiently high energies, all methods of calculating electronic stopping or cross sections converge. The energies of atomic binding become small compared to the energies transferred to the electrons by the projectile and free electron-like gases become an increasingly good approximation. Even more generally, the fact that the f-sum rule conserves oscillator strength in the loss function means that when you are integrating over all kinematically allowed dynamic variables (ω, q), any reasonable high-energy loss function contains most of its weight in a peak with most of the oscillator strength and the integration over this function erases the details of its structure, such that even plasmon pole models give similar values at high projectile energies. Thus, at speeds above a few atomic units (v_0), any calculations for the cross sections or stopping should be fairly reliable, with errors perhaps on the order of a few percent. This is consistent with our

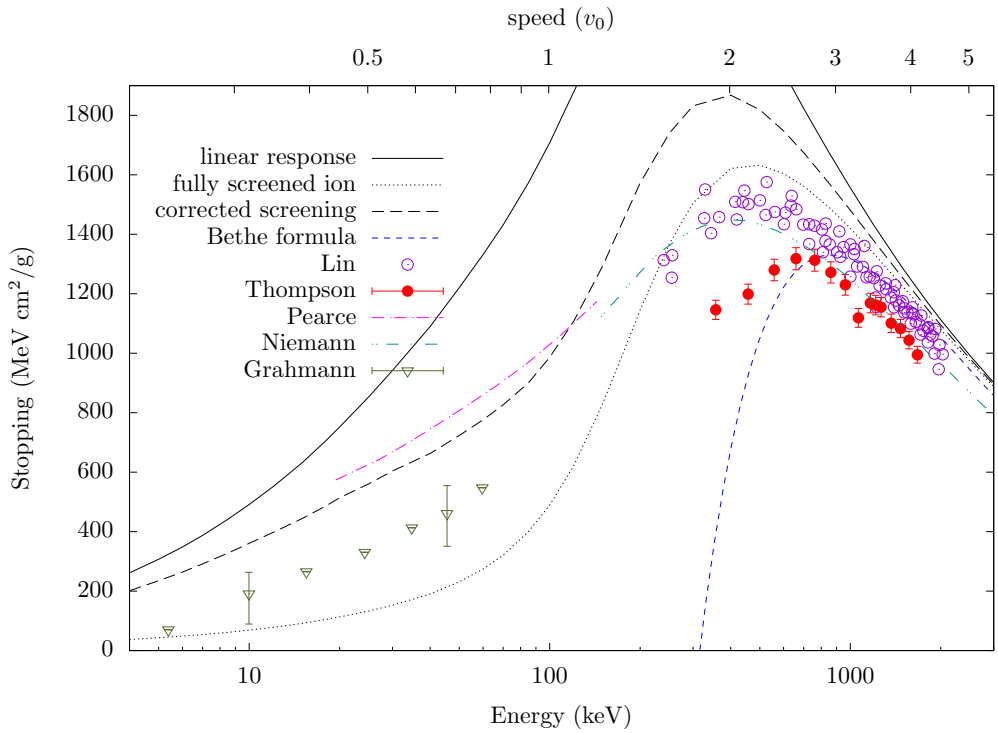

FIG. 5. Total predicted electronic stopping of α particles in silicon for basic linear response theory without ion screening (black solid line), with ion screening from all entrained electrons (black dotted line), with the corrected screening model (black long dashed line) compared to the Bethe (blue short dashed line) formula and to measured data by Lin *et al.* [41] (purple open circles); Thompson and Mackintosh [42] (red closed circles with error bars); Pearce and Hart [43] (magenta dot-long dashed line); Niemann *et al.* [44] (cyan double dot-long dashed line); and Grahmann and Kalbitzer [39] (dark green inverted open triangles). Of the measured data, only those of Grahmann and Kalbitzer are for electronic stopping; all others measure total stopping.

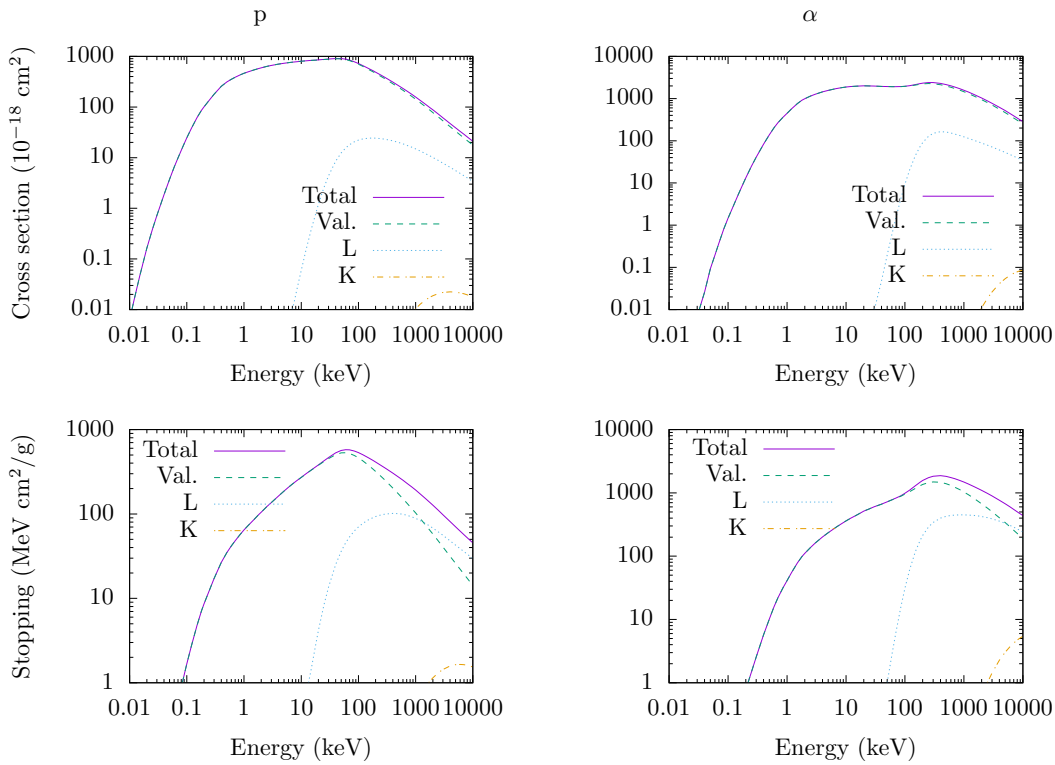

FIG. 6. Calculated contributions from valence (dashed line), L-shell (dotted line), and K-shell (dash-dot line) electrons, and the total of all electronic processes (solid line), to the electronic cross sections (above) and stopping (below) of protons (left) and α particles (right) in silicon. Proton valence results are from linear response, α particle valence results use the corrected screening method.

results, which approach the well-known Bethe stopping formula at high speeds, and generally are close to or within the available measured data. However, it must also be mentioned that the scattering and energy loss rate expressions were derived using a pure Coulomb potential and a longitudinal loss function and thus cannot be expected to hold at relativistic energies (at or above roughly the GeV scale for the light ions considered here).

The agreement of our predicted stopping with the data at high energies where L-shell excitations are expected to become important illustrates the applicability of the ECPSSR theory to stopping as well as to cross-section calculations and suggests that it gives a good overall description of the core excitation process by light ions. Using ECPSSR for core stopping can help ease the computational burdens of high-speed stopping calculations in general, including those using significantly different methods than the linear response used here.

This reasoning no longer holds as the projectile speed decreases and the material's electronic structure becomes increasingly reflected in the loss function. In addition, the screening of the ion by its entrained electrons reduces the response of the surrounding material. For protons, neglecting the entrained electrons gives results that are within a few percent of those of theories that allow bound states to form around the proton and take into account the electronic screening to all orders. In addition, the linear response stopping for a bare proton calculated using the *ab initio* loss function at lower energies and momentum transfers is in general agreement with the available experimental data on proton stopping in silicon, at between a few to roughly 20% deviation depending on the data set, with the exception of one data set which shows a deviation on the order of a factor of 2 from the theory and the other data at energies where they overlap. Consequently, we expect the accuracy of our method for calculating electronic loss rates, stopping, and cross sections to be within a few percent, at least for materials whose electronic properties are straightforward to calculate using modern electronic structure codes.

The situation with α particles is more complicated. A corrected screening model seems to be within a few percent accuracy at speeds above roughly 4 v_0 for the same reasons as for protons, before rising through a region of maximum discrepancy of about 20% error near 2 v_0 and then again approaching the experimental data at around 1 v_0 and below. As discussed, this model corrects linear response by explicitly adding a distributed charge cloud around the ion representing its bound electrons. But because the screening of a proton is well modeled by linear response, we need to remove the screening charge due to linear response from the charge cloud model. We do so by assuming that the linear response electronic screening distribution of a proton is similar to that of the modeled proton bound charge at the same speed, and subtracting off Z times the electron charge cloud of a proton. The other screening models considered for α particles in this paper cannot be recommended, as they either over- or underscreen the nucleus.

Silicon is a useful test material for models of this nature because of the ease of *ab initio* electronic structure calculations on silicon and the abundance of data on this material. Other materials made of light to midweight atoms would also be expected to work with this model if the material is amenable to DFT electronic structure methods. The model may break down for materials known to be strongly correlated, for example, at lower projectile energies, and materials with complicated structures may find the necessary electronic structure calculations to be time and computer resource intensive. As mentioned, the ECPSSR method for core excitations has only been developed for K, L, and M core shells. Heavier atoms with more core levels than this will require either additional work to derive the parameters for those shells or will need to represent the core states using the electronic structure method employed for the valence states.

The ability to simulate ion tracks will allow the understanding of material response to α decay as well as neutrons and the energetic ions their interactions produce. Such simulations can lead to increased understanding of the radiation track process and improved materials for radiation detection, including neutron-γ discrimination, or optimizing for speed or brightness in response to neutron interactions. It also may provide understanding of the signal produced by the recoil of atoms from other massive neutral particles and as such could be important to modeling the detector response in direct-detection searches for dark matter (see, e.g., Ref. [47]).

In summary, we have demonstrated a method that speeds up convergence of stopping calculations at high projectile energies, we have modified the computationally cheap ECPSSR method to obtain stopping due to core levels, and we present some preliminary evidence that a static model of entrained electrons of the projectile ion can include phenomena beyond linear response for ion stopping.

ACKNOWLEDGMENTS

Pacific Northwest National Laboratory (PNNL) is operated by Battelle for the U.S. Department of Energy (DOE) under Contract No. DE-AC05-76RL0-1830. Part of the research described in this paper was conducted under the Nuclear-physics, Particle-physics, Astrophysics, and Cosmology (NPAC) Initiative, a Laboratory Directed Research and Development effort at PNNL. This research was also supported in part by the National Nuclear Security Administration, Office of Defense Nuclear Nonproliferation Research and Development of the DOE. We would also like to acknowledge useful initial discussions with members of the SuperCDMS Collaboration regarding the detector response of silicon and germanium to nuclear recoils.

APPENDIX A: REVIEW OF SCREENING IN A CRYSTALLINE MATERIAL

Adler and Wiser [27,28] derived the longitudinal dielectric function of a crystalline material in the RPA to be

$$\epsilon_{\boldsymbol{K},\boldsymbol{K}'}(\boldsymbol{q}_B,\omega)=\delta_{\boldsymbol{K},\boldsymbol{K}'}-\frac{4\pi}{|\boldsymbol{q}||\boldsymbol{q}'|}\sum_{c}^{\text{un}}\sum_{v}^{\text{occ}}\int\frac{d^3k}{8\pi^3}\left[\frac{\rho_{cv}(\boldsymbol{k},\boldsymbol{q})\rho^*_{cv}(\boldsymbol{k},\boldsymbol{q}')}{\omega-\varepsilon_c(\boldsymbol{k})+\varepsilon_v(\boldsymbol{k}-\boldsymbol{q})+i\eta}-\frac{\rho_{vc}(\boldsymbol{k},\boldsymbol{q})\rho^*_{vc}(\boldsymbol{k},\boldsymbol{q}')}{\omega+\varepsilon_c(\boldsymbol{k})-\varepsilon_v(\boldsymbol{k}-\boldsymbol{q})+i\eta}\right]. \tag{A1}$$

Here, η is a positive infinitesimal, $\boldsymbol{K}$ and $\boldsymbol{K}'$ are reciprocal lattice vectors, the wave vector $\boldsymbol{q}_B$ is restricted to the first Brillouin zone, the summations are over unoccupied and occupied states, respectively, the integral is taken over the first Brillouin zone, and the density matrix elements are defined as

$$\rho_{nn'}(\boldsymbol{k},\boldsymbol{q})=\int d^3r\,\psi_{n,\boldsymbol{k}}(\boldsymbol{r})\,\psi^*_{n',\boldsymbol{k}-\boldsymbol{q}}(\boldsymbol{r})\,e^{-i\boldsymbol{q}\cdot\boldsymbol{r}}. \tag{A2}$$

In order to make the notation more compact, we use $\boldsymbol{q}=\boldsymbol{q}_B+\boldsymbol{K}$ and $\boldsymbol{q}'=\boldsymbol{q}_B+\boldsymbol{K}'$.

APPENDIX B: RATE OF LOSS DERIVATION

Consider an ion in a material. The ion moves with velocity $\boldsymbol{v}$ and has mass M and nuclear charge Z. The ion's position is $\boldsymbol{\mathcal{R}}=\boldsymbol{v}t$. Assume the ion has n bound electrons with a charge density $\rho_a(\boldsymbol{r}-\boldsymbol{v}t)$. If the Fourier transform of the static ion charge density is

$$\rho_a(\boldsymbol{q})=\int d^3r\,\rho_a(\boldsymbol{r})e^{-i\boldsymbol{q}\cdot\boldsymbol{r}}, \tag{B1}$$

then the Fourier transform of the moving ion charge density is found to be

$$\rho_a(\boldsymbol{q},\omega)=2\pi\,\rho_a(\boldsymbol{q})\,\delta(\boldsymbol{q}\cdot\boldsymbol{v}-\omega),\qquad M\to\infty. \tag{B2}$$

This result only holds in the limit of infinite ion mass, where the ion truly has a constant velocity. For finite mass, the energy-conserving δ function will need to include the effect of ion recoil

$$\rho_a(\boldsymbol{q},\omega)=2\pi\,\rho_a(\boldsymbol{q})\,\delta\left(\boldsymbol{q}\cdot\boldsymbol{v}-\frac{q^2}{2M}-\omega\right). \tag{B3}$$

The material is assumed to initially be in a product state $|\Phi_i\rangle$ of its electronic ground state $|\Psi_0\rangle$, a plane-wave state of the ion's center of mass $|\boldsymbol{p}\rangle$ with energy $|\boldsymbol{p}|^2/(2M)$, and the electronic state of the ion $|\Psi_a\rangle$. This section primarily focuses on excitations of the material electronic state with corresponding decreases in the kinetic energy of the ion; consequently, excitations of the ion electronic state will be neglected and the ion's charge can be treated as a classical quantity; $\langle\Psi_a|\check{\rho}_a(\boldsymbol{r})|\Psi_a\rangle=\rho_a(\boldsymbol{r})$, where $\check{\rho}_a$ is the charge density operator for the ion. The final states $|\Phi_f\rangle$ are likewise a product state of the final material electronic state with one or more particle-hole type excitations $|\Psi_e\rangle$, of a plane-wave state of the ion's center of mass $|\boldsymbol{p}'\rangle=|\boldsymbol{p}-\boldsymbol{q}\rangle$, and of the ion's charge distribution:

$$\begin{aligned}|\Phi_i\rangle&=|\Psi_0\rangle|\boldsymbol{p}\rangle|\Psi_a\rangle,\\ |\Phi_f\rangle&=|\Psi_e\rangle|\boldsymbol{p}'\rangle|\Psi_a\rangle.\end{aligned} \tag{B4}$$

The rate at which the system leaves its initial state and transitions to possible final states is given by Fermi's golden rule [48]

$$\Gamma(\boldsymbol{v})=2\pi\sum_f|\langle\Phi_f|H_{\text{int}}|\Phi_i\rangle|^2\delta(\omega_{if}), \tag{B5}$$

where ω_{if} is the energy difference between the state i and state f:

$$\omega_{if}=\omega_{0e}+\frac{|\boldsymbol{p}'|^2}{2M}-\frac{|\boldsymbol{p}|^2}{2M}=\omega_{0e}-\boldsymbol{q}\cdot\boldsymbol{v}+\frac{|\boldsymbol{q}|^2}{2M}. \tag{B6}$$

The interaction Hamiltonian is taken as the Coulomb interaction between the charge density of the ion and the material

$$H_{\text{int}}=\sum_{\boldsymbol{p}\boldsymbol{p}'}\sum_{\boldsymbol{K}}\int\frac{d^3q_B}{8\pi^3}\frac{4\pi}{|\boldsymbol{q}|^2}\rho^*_a(\boldsymbol{q})\check{\rho}(\boldsymbol{q})c^\dagger_{\boldsymbol{p}}c_{\boldsymbol{p}'}\,\delta(\boldsymbol{q}-\boldsymbol{p}+\boldsymbol{p}'), \tag{B7}$$

where $c_{\boldsymbol{p}}$ ($c^\dagger_{\boldsymbol{p}}$) is the destruction (creation) operator for the ion with momentum $\boldsymbol{p}$ and $\check{\rho}$ is the charge density operator for the electrons of the material

$$\check{\rho}(\boldsymbol{q})=-\sum_{nn'}\int\frac{d^3k}{8\pi^3}\,\rho_{nn'}(\boldsymbol{k},\boldsymbol{q})\,a^\dagger_{n',\boldsymbol{k}-\boldsymbol{q}}\,a_{n,\boldsymbol{k}}. \tag{B8}$$

Expanding the expression for the scattering rate obtains

$$\begin{aligned}\Gamma(\boldsymbol{v})=2\pi\sum_e\sum_{\boldsymbol{K}}\int\frac{d^3q_B}{8\pi^3}\left[\frac{4\pi}{|\boldsymbol{q}|^2}\right]^2|\rho_a(\boldsymbol{q})|^2\langle\Psi_0|\check{\rho}^\dagger(\boldsymbol{q})|\Psi_e\rangle\\ \times\langle\Psi_e|\check{\rho}(\boldsymbol{q})|\Psi_0\rangle\,\delta\left(\omega_{0e}-\boldsymbol{q}\cdot\boldsymbol{v}+\frac{|\boldsymbol{q}|^2}{2M}\right).\end{aligned} \tag{B9}$$

To make sense of this, we define a loss function $\mathcal{L}_{\boldsymbol{K}\boldsymbol{K}'}(\boldsymbol{q}_B,\omega)$ proportional to the anti-Hermitian component of the inverse dielectric function $\boldsymbol{\epsilon}^{-1(A)}_{\boldsymbol{K}\boldsymbol{K}'}(\boldsymbol{q}_B,\omega)$

$$\begin{aligned}\mathcal{L}_{\boldsymbol{K}\boldsymbol{K}'}(\boldsymbol{q}_B,\omega)&=-i\boldsymbol{\epsilon}^{-1(A)}_{\boldsymbol{K}\boldsymbol{K}'}(\boldsymbol{q}_B,\omega)\\ &=\frac{\epsilon^{-1}_{\boldsymbol{K}\boldsymbol{K}'}(\boldsymbol{q}_B,\omega)-\epsilon^{-1\dagger}_{\boldsymbol{K}\boldsymbol{K}'}(\boldsymbol{q}_B,\omega)}{2i},\end{aligned} \tag{B10}$$

which describes the strength of the different loss channels in the material for a given $\boldsymbol{q}$ and ω. In the free electron approximation, the loss function reduces to the scalar $\mathcal{L}(q,\omega)=\text{Im}\,\epsilon^{-1}(q,\omega)$. The normal methods of finding the inverse dielectric function using linear response of time-dependent perturbation theory [30,49] then gives

$$\begin{aligned}\boldsymbol{\epsilon}^{-1(A)}_{\boldsymbol{K}\boldsymbol{K}'}(\boldsymbol{q}_B,\omega)=\frac{-4i\pi^2}{|\boldsymbol{q}||\boldsymbol{q}'|}\sum_e[\langle\Psi_0|\check{\rho}(\boldsymbol{q})|\Psi_e\rangle\langle\Psi_e|\check{\rho}^\dagger(\boldsymbol{q}')|\Psi_0\rangle\\ \times\delta(\omega-\omega_{0e})-\langle\Psi_0|\check{\rho}^\dagger(\boldsymbol{q}')|\\ \times\Psi_e\rangle\langle\Psi_e|\check{\rho}(\boldsymbol{q})|\Psi_0\rangle\delta(\omega+\omega_{0e})]\end{aligned} \tag{B11}$$

so that

$$\Gamma(\boldsymbol{v})=2\int_0^\infty d\omega\sum_{\boldsymbol{K}}\int\frac{d^3q_B}{8\pi^3}\,\frac{4\pi}{|\boldsymbol{q}|^2}\,|\rho_a(\boldsymbol{q})|^2\mathcal{L}_{\boldsymbol{K}\boldsymbol{K}}(\boldsymbol{q}_B,\omega)\,\delta$$

$$\times \left(\omega - \boldsymbol{q}\cdot\boldsymbol{v} + \frac{|\boldsymbol{q}|^2}{2M}\right). \tag{B12}$$

The rate of energy transfer from the projectile ion to the material is easily found by weighting the integrand in the scattering rate expression by the energy transfer ω

$$\dot{E}(\boldsymbol{v}) = 2\int_0^\infty d\omega\,\omega \sum_{\boldsymbol{K}} \int \frac{d^3q_B}{8\pi^3}\,\frac{4\pi}{|\boldsymbol{q}|^2}\,|\rho_a(\boldsymbol{q})|^2 \mathcal{L}_{\boldsymbol{KK}}(\boldsymbol{q}_B,\omega)\,\delta \times \left(\omega - \boldsymbol{q}\cdot\boldsymbol{v} + \frac{|\boldsymbol{q}|^2}{2M}\right). \tag{B13}$$

In other words, the rate of excitations is a sum over the rates of individual energy and momentum transfers, given by the Coulomb interaction of the radiation particle with the available loss channels of the material.

APPENDIX C: REVIEW OF ECPSSR METHOD

The PWBA expression for the cross section is traditionally written as

$$\sigma_J = \sigma_{0J}\,\theta_J^{-1}\,F_J(\eta_J/\theta_J^2,\theta_J), \tag{C1}$$

where $J = K, L1, L2, L3, M1, \ldots$ references the core state being ionized,

$$\sigma_{0J} = 8\pi Z^2 Z_J^{-4}, \tag{C2}$$

Z_J is the charge of the target ion modified for the electronic screening of other core shells using the method of Slater [50],

$$\theta_J = \frac{2\,\omega_J}{Z_J^2}, \tag{C3}$$

ω_J is the core shell binding energy, and

$$\eta_J = \left(\frac{v}{Z_J}\right)^2. \tag{C4}$$

The quantity $F_J(\eta_J/\theta_J^2,\theta_J)$ is a universal core cross-section integral, which can be computed using

$$F_J(\eta_J/\theta_J^2,\theta_J) = \frac{\theta_J}{\eta_J} f_J, \tag{C5}$$

$$f_J = \int_{W_{\min}}^{W_{\max}} dW \int_{Q_{\min}}^{Q_{\max}} dQ |G_{W,J}|^2. \tag{C6}$$

The integration variable W is the scaled energy transfer and Q is the scaled momentum transfer

$$W = \frac{2\,\omega}{Z_J^2}, \tag{C7}$$

$$Q = \frac{q^2}{Z_J^2}. \tag{C8}$$

The functional form of $G_{W,J}$ depends on the core shell being ionized [51,52]; the interested reader can find the specifics in the referenced literature. For our purposes, it suffices to note that the rate of energy loss of the ion to excitations of the specific core level can be calculated under the same approximation by weighting the scaled energy integral by $Z_J^2 W/2$. This allows us to calculate the stopping of core levels using Eq. (6). The ECPSSR corrections used for the cross sections can just as well be used for stopping calculations.

At this time, the authors are only aware of published forms of $G_{W,J}$ for K, L, and M shells. If this method is to be used for materials containing atoms heavier than Kr, additional work will be required to determine the expression of PWBA cross sections for N, O, and P shells.

[1] S. Agostinelli, J. Allison, K. Amako, J. Apostolakis, H. Araujo, P. Arce, M. Asai, D. Axen, S. Banerjee, G. Barrand, F. Behner, L. Bellagamba, J. Boudreau, L. Broglia, A. Brunengo, H. Burkhardt, S. Chauvie, J. Chuma, R. Chytracek, G. Cooperman, G. Cosmo, P. Degtyarenko, A. Dell'Acqua, G. Depaola, D. Dietrich, R. Enami, A. Feliciello, C. Ferguson, H. Fesefeldt, G. Folger, F. Foppiano, A. Forti, S. Garelli, S. Giani, R. Giannitrapani, D. Gibin, J. Gómez Cadenas, I. González, G. Gracia Abril, G. Greeniaus, W. Greiner, V. Grichine, A. Grossheim, S. Guatelli, P. Gumplinger, R. Hamatsu, K. Hashimoto, H. Hasui, A. Heikkinen, A. Howard, V. Ivanchenko, A. Johnson, F. Jones, J. Kallenbach, N. Kanaya, M. Kawabata, Y. Kawabata, M. Kawaguti, S. Kelner, P. Kent, A. Kimura, T. Kodama, R. Kokoulin, M. Kossov, H. Kurashige, E. Lamanna, T. Lampén, V. Lara, V. Lefebure, F. Lei, M. Liendl, W. Lockman, F. Longo, S. Magni, M. Maire, E. Medernach, K. Minamimoto, P. Mora de Freitas, Y. Morita, K. Murakami, M. Nagamatu, R. Nartallo, P. Nieminen, T. Nishimura, K. Ohtsubo, M. Okamura, S. O'Neale, Y. Oohata, K. Paech, J. Perl, A. Pfeiffer, M. Pia, F. Ranjard, A. Rybin, S. Sadilov, E. Di Salvo, G. Santin, T. Sasaki, N. Savvas, Y. Sawada, S. Scherer, S. Sei, V. Sirotenko, D. Smith, N. Starkov, H. Stoecker, J. Sulkimo, M. Takahata, S. Tanaka, E. Tcherniaev, E. Safai Tehrani, M. Tropeano, P. Truscott, H. Uno, L. Urban, P. Urban, M. Verderi, A. Walkden, W. Wander, H. Weber, J. Wellisch, T. Wenaus, D. Williams, D. Wright, T. Yamada, H. Yoshida, and D. Zschiesche, Nucl. Instr. Methods Phys. Res. Sec. A **506**, 250 (2003).

[2] C. J. Werner, MCNP Users Manual, Code Version 6.2, Report LA-UR-18-20808, Los Alamos National Laboratory, NM, 2017.

[3] H. Bethe, Ann. Phys. **397**, 325 (1930).

[4] J. Lindhard and M. Sharff, Phys. Rev. **124**, 128 (1961).

[5] J. P. Biersack and L. G. Haggmark, Nucl. Instrum. Methods **174**, 257 (1980).

[6] J. F. Ziegler, J. Appl. Phys. **85**, 1249 (1999).

[7] I. Campillo, J. M. Pitarke, and A. G. Eguiluz, Phys. Rev. B **58**, 10307 (1998).

[8] I. Campillo, J. M. Pitarke, A. G. Eguiluz, and A. García, Nucl. Instrum. Methods Phys. Res. B **135**, 103 (1998).

[9] J. M. Pitarke and I. Campillo, Nucl. Instrum. Methods Phys. Res. B **164–165**, 147 (2000).

[10] A. A. Shukri, F. Bruneval, and L. Reining, Phys. Rev. B **93**, 035128 (2016).

[11] P. M. Echenique, R. M. Nieminen, J. C. Ashley, and R. H. Ritchie, Phys. Rev. A **33**, 897 (1986).

[12] V. U. Nazarov, J. M. Pitarke, C. S. Kim, and Y. Takada, Phys. Rev. B **71**, 121106(R) (2005).

[13] V. U. Nazarov, J. M. Pitarke, Y. Takada, G. Vignale, and Y.-C. Chang, Phys. Rev. B **76**, 205103 (2007).

[14] V. U. Nazarov, J. M. Pitarke, Y. Takada, G. Vignale, and Y.-C. Chang, Int. J. Mod. Phys. B **22**, 3813 (2008).

[15] J. M. Pruneda, D. Sánchez-Portal, A. Arnau, J. I. Juaristi, and E. Artacho, Phys. Rev. Lett. **99**, 235501 (2007).

[16] D. C. Yost and Y. Kanai, Phys. Rev. B **94**, 115107 (2016).

[17] D. C. Yost, Y. Yao, and Y. Kanai, Phys. Rev. B **96**, 115134 (2017).

[18] W. Brandt and G. Lapicki, Phys. Rev. A **23**, 1717 (1981).

[19] W. Brandt and M. Kitagawa, Phys. Rev. B **25**, 5631 (1982).

[20] R. J. Mathar and M. Posselt, Phys. Rev. B **51**, 107 (1995).

[21] M. P. Prange, Y. Xie, L. W. Campbell, F. Gao, and S. Kerisit, J. Appl. Phys. **122**, 234504 (2017).

[22] F. Gao, Y. Xie, S. Kerisit, L. W. Campbell, and W. J. Weber, Nucl. Instrum. Methods Phys. Res. A **652**, 564 (2011).

[23] F. Gao, Y. Xie, Z. Wang, S. Keresit, D. Wu, L. W. Campbell, R. M. Van Ginhoven, and M. P. Prange, J. Appl. Phys. **114**, 173512 (2013).

[24] X. Gonze, B. Amadon, P. M. Anglade, J. M. Beuken, F. Bottin, P. Boulanger, F. Bruneval, D. Caliste, R. Caracas, M. Cote, T. Deutsch, L. Genovese, P. Ghosez, M. Giantomassi, S. Goedecker, D. Haman, P. Hermet, F. Jollet, G. Jomard, S. Leroux, M. Mancini, S. Mazevet, M. J. T. Oliveira, G. Onida, Y. Pouillon, T. Rangel, G. M. Rignanese, D. Sangalli, R. Shaltaf, M. Torrent, M. J. Verstraete, G. Zérah, and J. W. Zwanziger, Comput. Phys. Commun. **180**, 2582 (2009).

[25] G. Kresse and J. Furthmüller, Phys. Rev. B **54**, 11169 (1996).

[26] M. Valiev, E. J. Bylaska, N. Govind, K. Kowalski, T. P. Straatsma, H. J. J. van Dam, D. Wang, J. Nieplocha, E. Apra, T. L. Windus, and W. A. de Jong, Comput. Phys. Commun. **181**, 1477 (2010).

[27] S. L. Adler, Phys. Rev. **126**, 413 (1962).

[28] N. Wiser, Phys. Rev. **129**, 62 (1963).

[29] J. Lindhard, Det Kongelige Danske Videnskabernes Selskab Matematisk-fysiske Meddelelser **28**, 1 (1954).

[30] G. D. Mahan, *Many-Particle Physics*, 2nd ed. (Plenum, New York, 1990), Chap. 5, Sec. 5.5.B.

[31] Many authors call this the stopping *power*. However, because it has units of force rather than power, we do not use this terminology.

[32] D. R. Hamann, Phys. Rev. B **88**, 085117 (2013).

[33] G. Lehmann and M. Taut, Phys. Status Solidi B **54**, 469 (1972).

[34] C. D. Archubi and N. R. Arista, Phys. Rev. A **96**, 062701 (2017).

[35] H. Tawara, Y. Hachiya, K. Ishii, and S. Morita, Phys. Rev. A **13**, 572 (1976).

[36] W. M. Ariyasinghe, H. T. Awuku, and D. Powers, Phys. Rev. A **42**, 3819 (1990).

[37] E. Kührt, K. Lenkeit, and F. Täubner, Phys. Status Solidi A **66**, K131 (1981).

[38] P. Mertens and P. Bauer, Nucl. Instrum. Methods Phys. Res. B **33**, 133 (1988).

[39] H. Grahmann and S. Kalbitzer, Nucl. Instrum. Methods **132**, 119 (1976).

[40] S. Z. Izmailov, E. I. Sirotinin, and A. F. Tulinov, Nucl. Instrum. Methods **168**, 81 (1980).

[41] W. K. Lin, H. G. Olson, and D. Powers, J. Appl. Phys. **44**, 3631 (1973).

[42] D. A. Thompson and W. D. Mackintosh, J. Appl. Phys. **42**, 3969 (1971).

[43] J. D. Pearce and R. R. Hart, J. Appl. Phys. **52**, 5056 (1981).

[44] D. Niemann, G. Konac, and S. Kalbitzer, Nucl. Instrum. Methods Phys. Res. B **118**, 11 (1996).

[45] M. J. Berger, J. S. Coursey, M. A. Zucker, and J. Chang, Pstar, https://physics.nist.gov/PhysRefData/Star/Text/PSTAR.html.

[46] M. J. Berger, J. S. Coursey, M. A. Zucker, and J. Chang, Astar, https://physics.nist.gov/PhysRefData/Star/Text/ASTAR.html.

[47] R. Agnese, A. J. Anderson, T. Aramaki, I. Arnquist, W. Baker, D. Barker, R. Basu Thakur, D. A. Bauer, A. Borgland, M. A. Bowles, P. L. Brink, R. Bunker, B. Cabrera, D. O. Caldwell, R. Calkins, C. Cartaro, D. G. Cerdeño, H. Chagani, Y. Chen, J. Cooley, B. Cornell, P. Cushman, M. Daal, P. C. F. Di Stefano, T. Doughty, L. Esteban, S. Fallows, E. Figueroa-Feliciano, M. Fritts, G. Gerbier, M. Ghaith, G. L. Godfrey, S. R. Golwala, J. Hall, H. R. Harris, T. Hofer, D. Holmgren, Z. Hong, E. Hoppe, L. Hsu, M. E. Huber, V. Iyer, D. Jardin, A. Jastram, M. H. Kelsey, A. Kennedy, A. Kubik, N. A. Kurinsky, A. Leder, B. Loer, E. Lopez Asamar, P. Lukens, R. Mahapatra, V. Mandic, N. Mast, N. Mirabolfathi, R. A. Moffatt, J. D. Morales Mendoza, J. L. Orrell, S. M. Oser, K. Page, W. A. Page, R. Partridge, M. Pepin, A. Phipps, S. Poudel, M. Pyle, H. Qiu, W. Rau, P. Redl, A. Reisetter, A. Roberts, A. E. Robinson, H. E. Rogers, T. Saab, B. Sadoulet, J. Sander, K. Schneck, R. W. Schnee, B. Serfass, D. Speller, M. Stein, J. Street, H. A. Tanaka, D. Toback, R. Underwood, A. N. Villano, B. von Krosigk, B. Welliver, J. S. Wilson, D. H. Wright, S. Yellin, J. J. Yen, B. A. Young, X. Zhang, and X. Zhao (SuperCDMS collaboration), Phys. Rev. D **95**, 082002 (2017).

[48] J. J. Sakurai, *Modern Quantum Mechanics* (Addison Wesley, Reading, MA, 1994).

[49] D. Pines, *Elementary Excitations in Solids* (Perseus, Reading, MA, 1999).

[50] J. C. Slater, Phys. Rev. **36**, 57 (1930).

[51] O. Benka and A. Kropf, At. Data Nucl. Data Tables **22**, 219 (1978).

[52] B. H. Choi, Phys. Rev. A **7**, 2056 (1973).